

Expanded View Figures

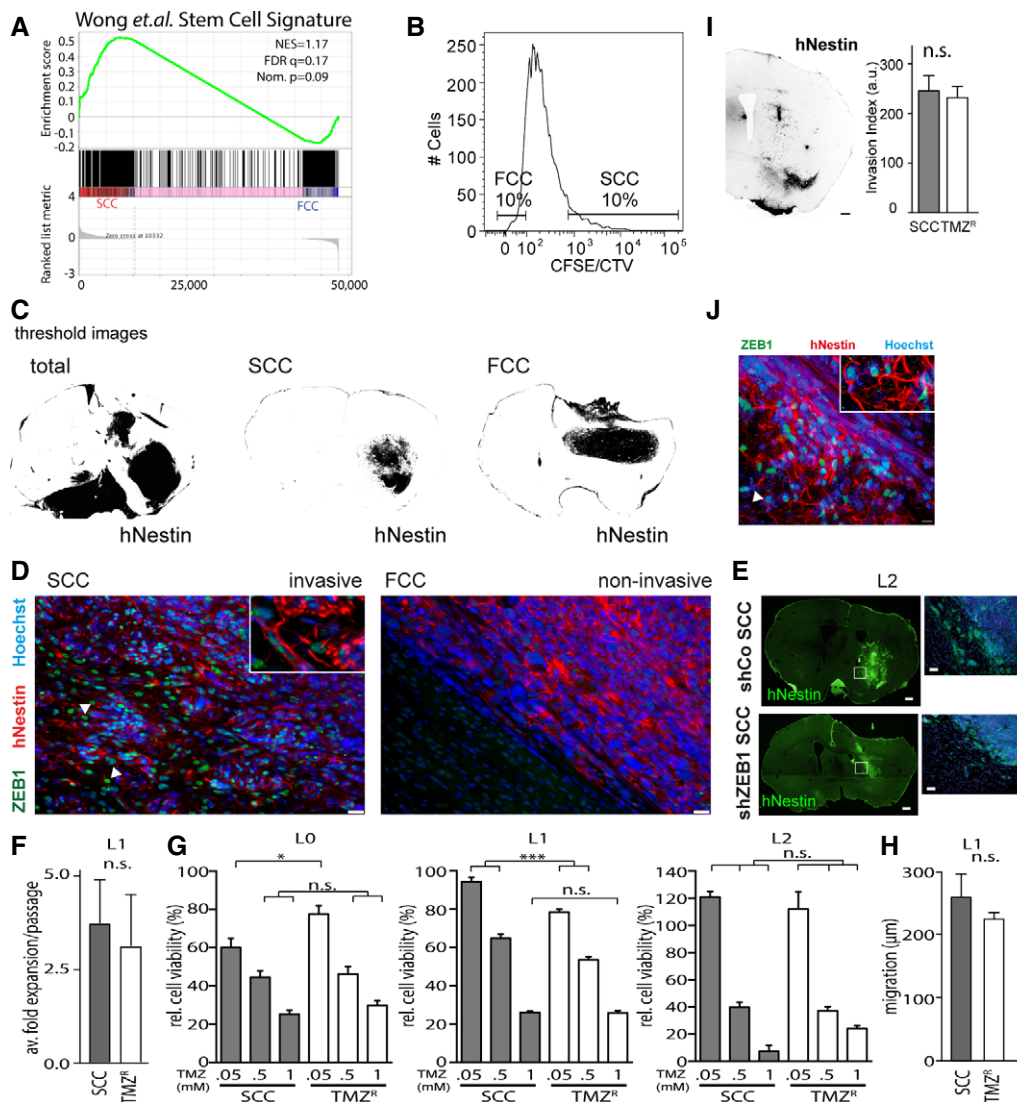


Figure EV1. Invasion and chemoresistance properties in SCCs.

- A GSEA of SCC ($n = 3$ biological replicates, L0-1-2) and FCC ($n = 3$ biological replicates, L0-1-2) RNA seq data sets for enrichment of the stem cell gene signature (Wong *et al.*, 2008). FDR, false discovery rate; NES, normalized enrichment score; Nom., nominal.
- B SCCs and FCCs were separated 6–8 days after (CFSE or CTV) CellTrace loading. Gates were set as 10% CellTrace^{hi} versus CellTrace^{lo}.
- C Threshold images of human-specific nestin staining were used for quantification of tumor invasion ($n = 5$ animals per group, see Materials and Methods).
- D Immunofluorescence imaging revealed notable differences between invasive/SCC-derived, and non-invasive/FCC-derived, tumors. Invasive SCC-derived tumors were positive for ZEB1 (green), while this marker was absent in the tumor masses derived from FCCs. Tumor cells were labeled with hNestin (red) and nuclei with Hoechst (blue). Scale bars, 10 μm. Arrowheads indicate infiltrative Zeb1⁺ GBM cells.
- E Fluorescence imaging showed that the invasion of ZEB1 knockdown (shZEB1) SCC-derived tumors from orthotopic xenografts was greatly reduced compared to that of control SCC-derived tumors (shCo). Scale bars, 10 μm.
- F–J Temozolomide-resistant cells (TMZ^R) and SCCs derived from the L1 patient-derived GBM line displayed similar growth rates ($n = 3$) (F), TMZ sensitivities ($n = 6–8$, $*P < 0.05$, $***P < 0.001$, one-way ANOVA with Tukey post-test) (G), as well as migration (H) and invasion capabilities (scale bars, 500 μm) (I) ($n = 3–12$). These results were accompanied by the detection of high expression levels of ZEB1 in TMZ^R-derived tumors. The arrowhead indicates infiltrative Zeb1⁺ GBM cell (J). Values are mean ± SEM.

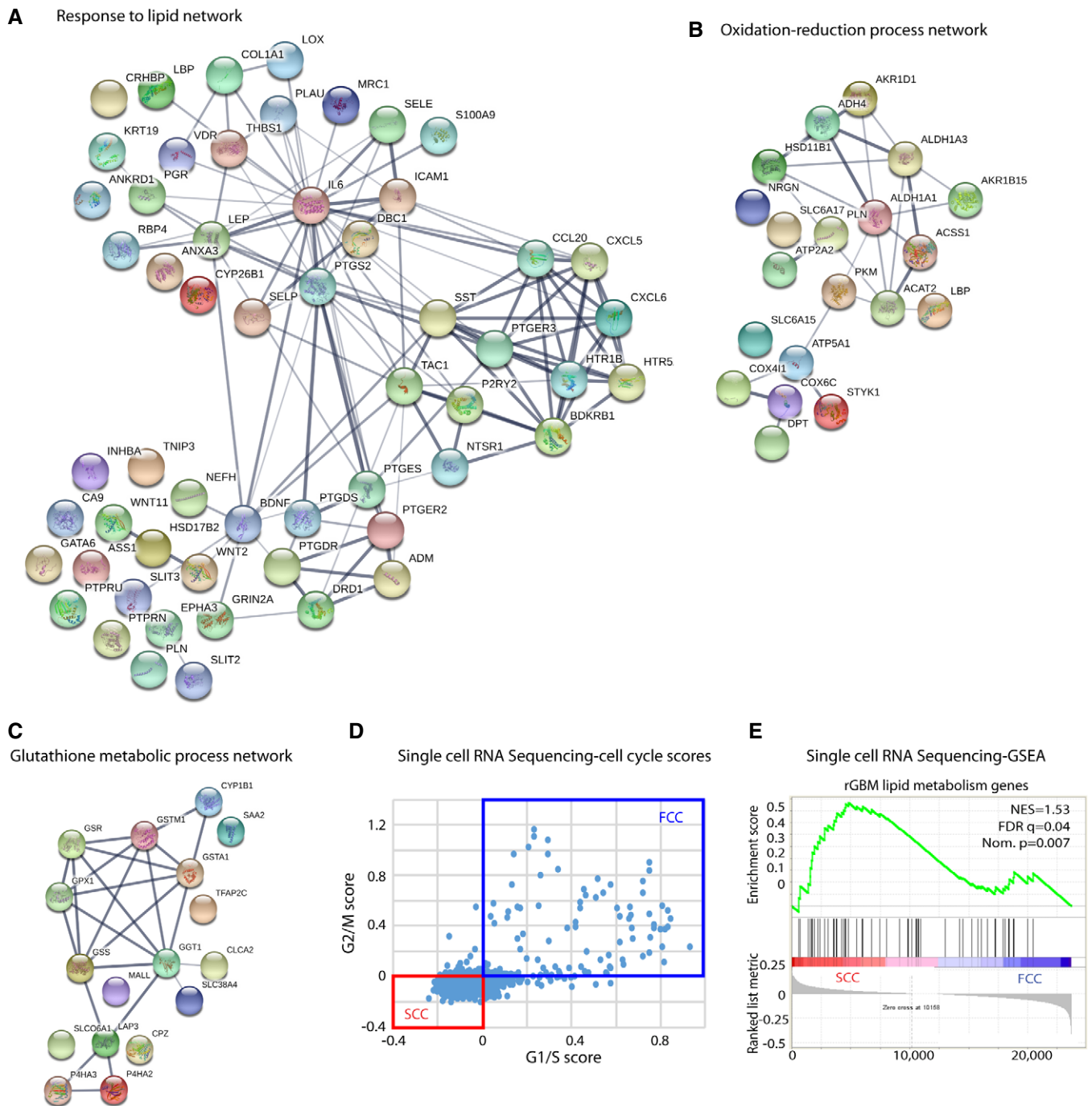


Figure EV2. Differentially regulated pathways between SCCs and FCCs.

A The use of Search Tool in the Retrieval of Interacting Genes/Proteins database (STRING) indicated an overrepresentation of genes associated with lipid metabolism in recurrent GBMs. Red nodes designate the response to lipid genes ($n = 56$) that are significantly overexpressed in recurrent GBMs within the entire network of genes.

B, C Gene networks involved in oxidation–reduction (B) and antioxidant processes (C) are up-regulated in recurrent tumors.

D Cells from single-cell RNA sequencing data were classified into slow- (SCC) and fast-cycling (FCC) clusters based on the relative expression of cell cycle G1/S (x-axis) and G2/M (y-axis)-associated gene sets.

E GSEA of SCC ($n = 3$ biological replicates, LO-1-2) and FCC ($n = 3$ biological replicates, LO-1-2) RNA seq data sets for enrichment of the lipid gene signature identified in TCGA rGBM and our three GBM-derived SCCs. FDR, false discovery rate; NES, normalized enrichment score; Nom., nominal.

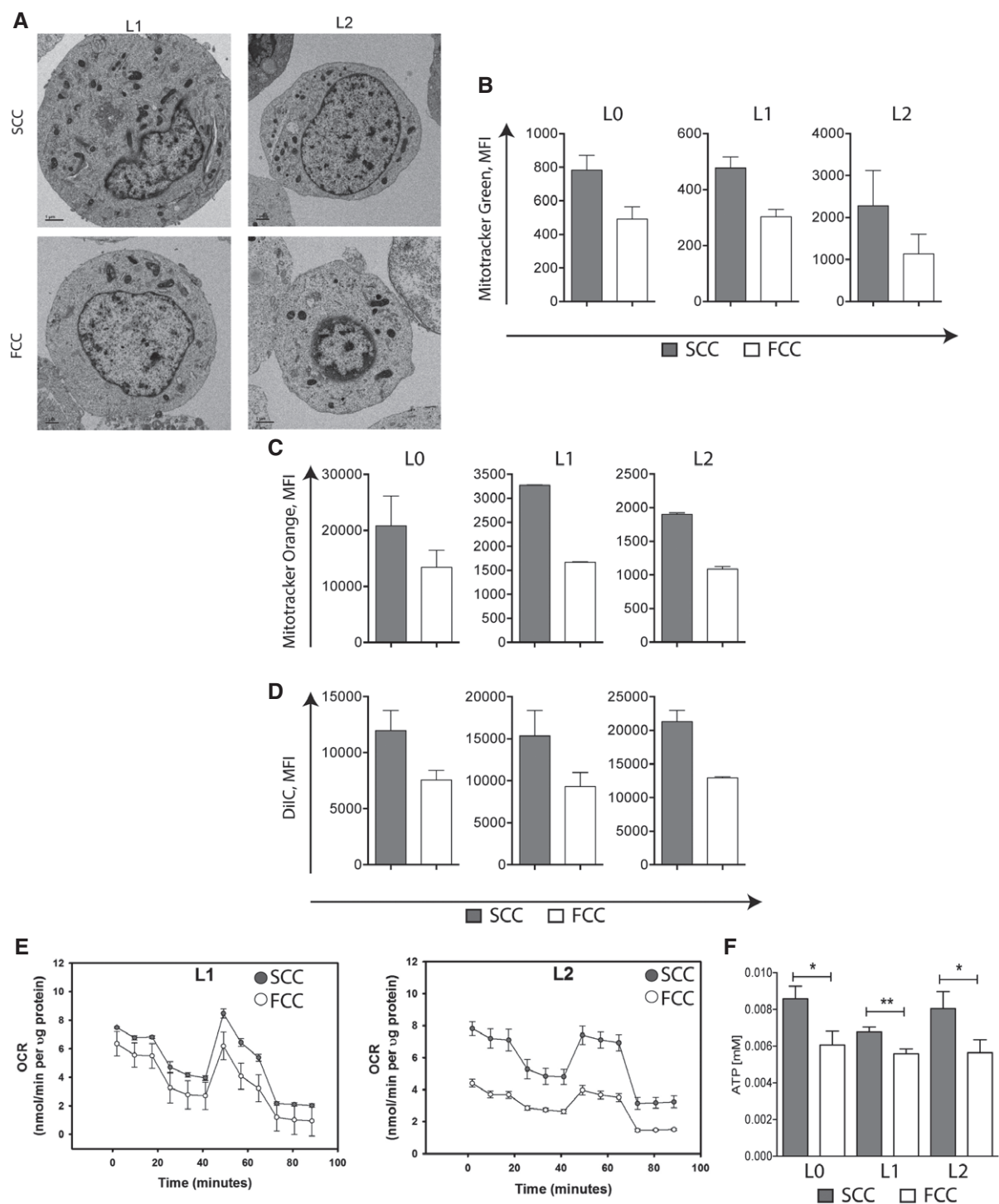


Figure EV3. SCCs and FCCs show different mitochondrial properties.

- A** Electron microscopy images of SCCs and FCCs from L1 and L2 patient-derived GBM cell lines showing greater number of mitochondria in SCCs than FCCs. Scale bar, 1 μ m.
- B** Raw values of mean fluorescence intensity (MFI) following MitoTracker Green staining in SCCs and FCCs derived from hGBM L0 ($n = 10$), L1 ($n = 13$), and L2 ($n = 6$). Values are mean \pm SEM.
- C** Raw values of mean fluorescence intensity (MFI) following MitoTracker Orange staining in SCCs and FCCs (mean \pm SEM, L0, $n = 9$; L1, $n = 2$; L2, $n = 6$).
- D** Raw values of mean fluorescence intensity (MFI) in SCCs and FCCs following the MitoProbe DiIC1 assay (mean \pm SEM, L0, $n = 4$; L1, $n = 2$; L2, $n = 5$).
- E, F** Oxygen consumption rate (OCR) measured using the XF Cell Mito Stress Assay (**E**) and ATP production measured using the luciferase-based ATP-lite assay (**F**) in SCCs and FCCs (mean \pm SEM, L0, $n = 18$; L1, $n = 15$; L2, $n = 15$, * $P < 0.05$, ** $P < 0.01$, t-test).

Figure EV4. FABPs in glioma and SCCs.

- A, B FABP7 protein expression in normal brain tissue (A) and glioma (B). Image credit: Human Protein Atlas v16.1, www.proteinatlas.org.
- C GSEA of SCC ($n = 3$ biological replicates, LO-1-2) and FCC ($n = 3$ biological replicates, LO-1-2) RNA seq data sets for enrichment of FABP7-correlated genes. FDR, false discovery rate; NES, normalized enrichment score; Nom., nominal.
- D C16-BODIPY uptake in control conditions or with 250 nM of FABP3 inhibitor (BMS309403; mean \pm SEM, $n = 3$, *** $P < 0.0001$, linear regression).
- E FACS of least and most intense GFP-positive single cells and representative immunofluorescence microscopy images of FABP7 immunoreactivity in wild-type (clone D5 WT) and crFABP7 (clone H7) clones following CRISPR/Cas9 plasmid transfection for FABP7. FABP7 fluorescence mean intensity (FMI) was higher in wild-type than crFABP7 clones as measured by flow cytometry. FABP7 expression was assessed using two different antibodies (clone AF3166 and clone sc-300-88). Nuclei were labeled with DAPI.

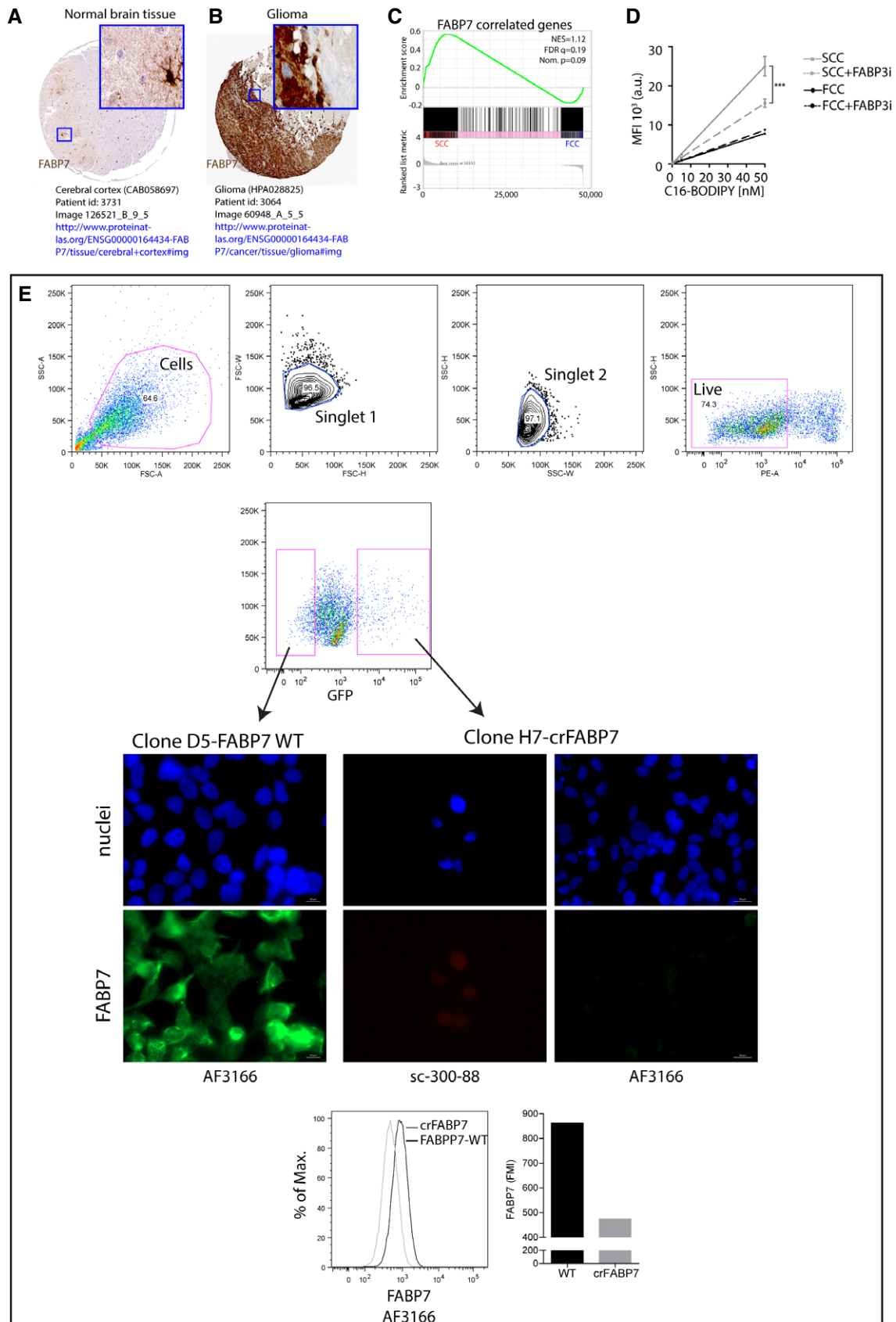


Figure EV4.

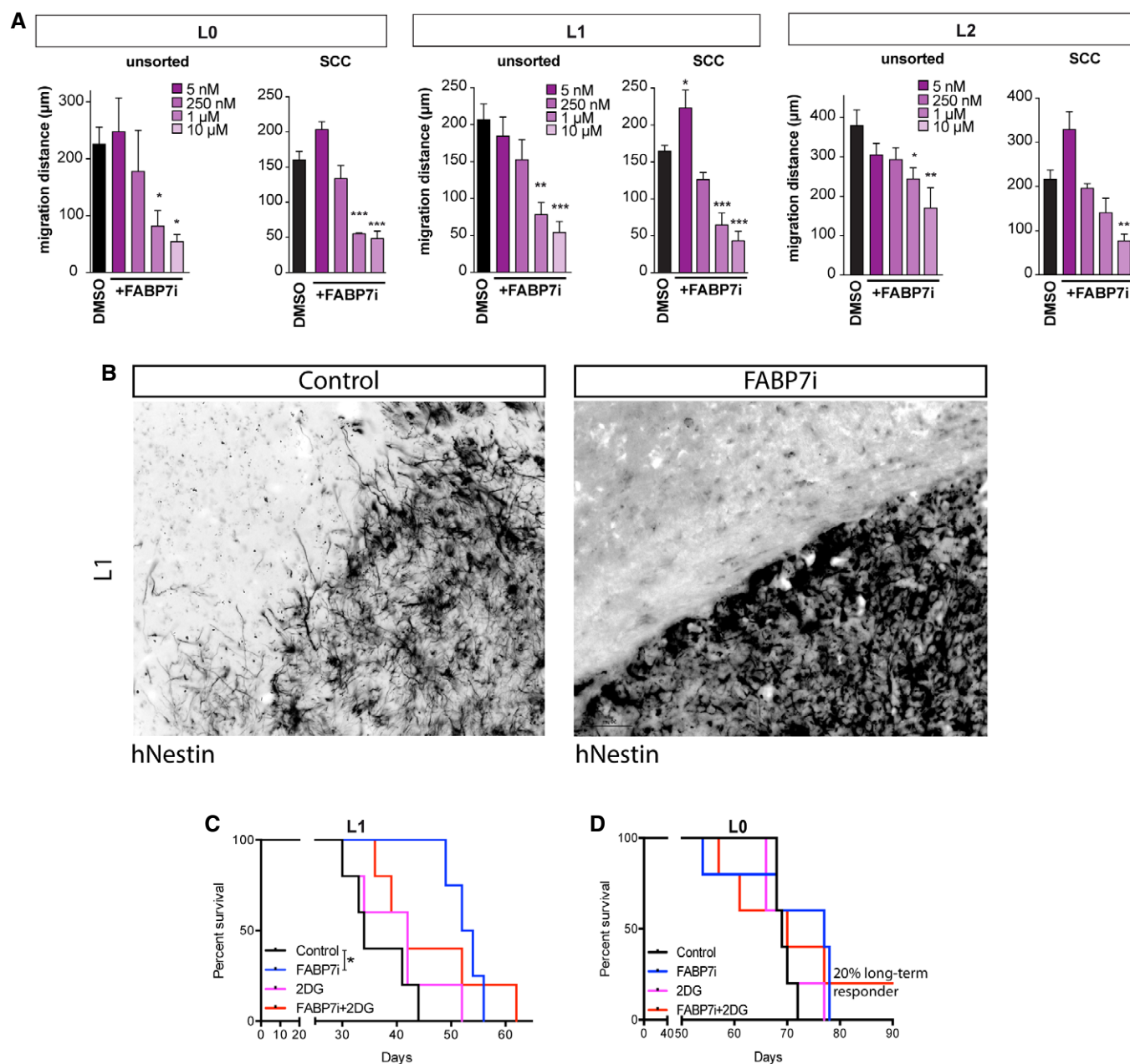


Figure EV5. Role of FABP7 in SCCs' infiltration and resistance to glycolysis inhibition.

- A Total and SCC populations were treated with FABP7i concentrations ranging from 5 nM to 10 μ M. In L0 and L1, 1 and 10 μ M concentrations of FABP7i significantly reduced the migration distances of overall unsorted and SCC populations, whereas only 10 μ M FABP7i was significant for L2 SCC ($n = 3$, mean \pm SEM, $*P < 0.05$, $**P < 0.001$, $***P < 0.0005$, one-way ANOVA with Tukey post-test).
- B *In vivo* inhibition of FABP7 also resulted in decreased tumor cell invasion. Scale bar, 50 μ m.
- C, D The effects of FABP7 inhibition, alone or in combination with pharmacological targeting of glycolysis with 2-DG, were conducted on tumors derived from the xenotransplants of L1 ($n = 4-5$) (C) and L0 ($n = 5-6$) (D) GBM patient-derived cells lines. $*P < 0.05$, log-rank test.